

Forming and Crash Induced Damage Evolution and Failure Prediction Part 2: A comparison of damage models

Frieder Neukamm
Universität Stuttgart

Markus Feucht
DaimlerChrysler AG, Sindelfingen

André Haufe
Dynamore GmbH, Stuttgart

Abstract:

With increasing requirements on crashworthiness, and light-weight car body structures being a central issue in future automotive development, the use of high strength steel qualities has become widespread in modern cars. Since these materials often show significantly lower ductility than conventional steels, it is of great importance to precisely predict failure under crash loading conditions.

It seems more and more evident that the before going treatment of the material through the process chain of rolling to forming significantly influences crash performance of the respective material. An emphasis has been laid on identification of damage parameters and a comparison of relevant damage accumulation models and theories from forming to crash simulation.

Special attention was paid to existing differences regarding stress states between forming and crash loading, to clarify differences in failure prediction models respectively. Numerical simulations of Nakazima tests using solid elements were conducted, to get an impression of stress states in these tests used for the determination of Forming Limit Diagrams (FLD). A review of literature and own considerations are shown, to describe a formulation of failure strains dependent on the third invariant of the stress tensor or the Lode angle. Several possibilities to consistently describe damage and failure in both forming and crash simulations are considered.

Keywords:

Damage models, Crash simulation, Lode dependence

1 Introduction

Increasing requirements on crashworthiness, together with an ever-growing interest in weight reduction, lead to development and increasing use of advanced materials in car body structures. In addition to classic light-weight materials such as aluminium and Al-Mg alloys, advanced high strength steels are at present used in a wide range of car body structures. Representing a rather new class of steel materials, a better understanding of the behaviour of these materials under forming and crash loading is of great interest for car manufacturers.

Most of these materials show significantly lower ductility than conventional deep-draw steels, hence crack development has to be expected in crash situations. Due to this fact, a sufficiently precise prediction of failure is becoming more and more important in crash simulations. For this purpose, it has been proved necessary to take into account the process chain of manufacturing of the respective part. Especially forming processes can considerably alter mechanical properties of the respective part.

Since the use of forming simulations is common practise, one main objective of the present work is to consider a consistent damage formulation which can be used to calculate the local pre-damage from forming, and that allows for a direct transfer of this damage parameter to the corresponding crash simulation.

2 Differences in damage models – forming vs. crash

To get an idea of differences in damage models, it should be considered how failure is defined in forming simulations and in crash simulations. For forming purposes, failure is often considered as the point of initial instability, or the onset of necking. The conventional approach to this is to determine the critical strains by denoting the respective elements in a Forming Limit Diagram (FLD).

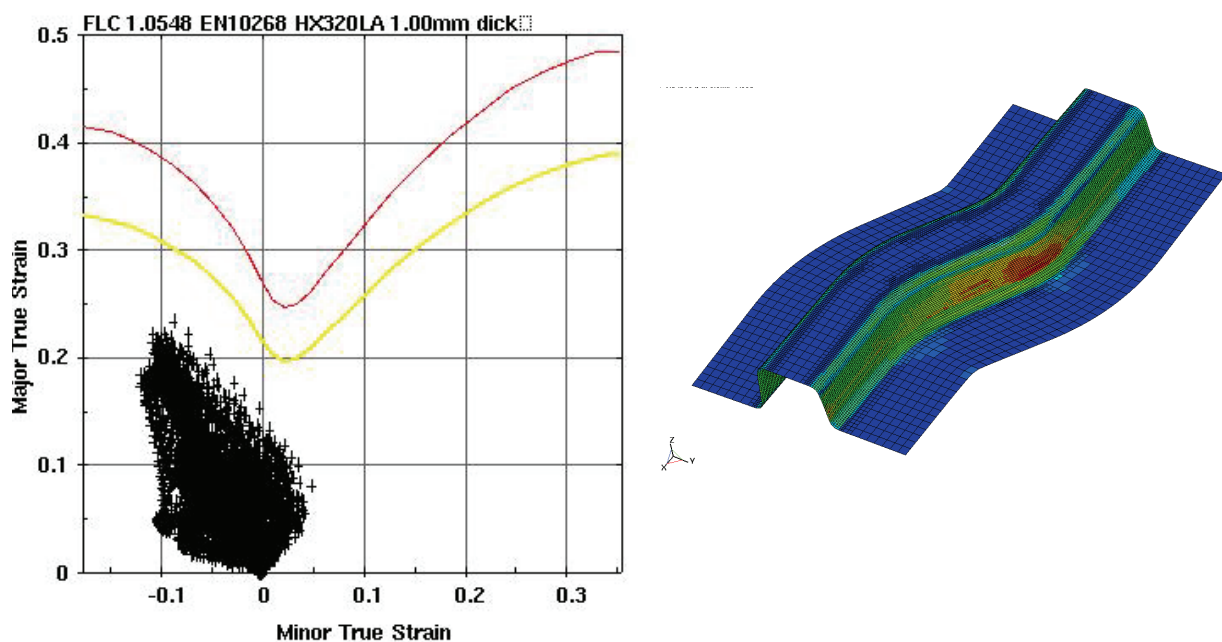


Figure 1: a.) Forming Limit Diagram

b.) S-Rail Forming Simulation

In Forming Limit Diagrams, major true strains vs. minor true strains are denoted. It shows the variation of ductility with changing ratio of major strains. However, it does not take into account a possible variation of strain states during the forming process. Only the final ratio of strains is considered, and taken as a measure of damage in relation to the limit strain for a distinct strain ratio.

Damage measure in crash simulations mostly follows fundamentally different ideas: based on stresses rather than strains, several different damage models are in use. Most of these models define fracture strain as a function of stress triaxiality $\eta = \sigma_m / \sigma_e$, where

$$\sigma_m = -\frac{\sigma_{kk}}{3} = -\frac{\sigma_1 + \sigma_2 + \sigma_3}{3} \quad \text{Hydrostatic pressure}$$

$$\sigma_e = \sqrt{\frac{1}{2}[(\sigma_1 - \sigma_2)^2 + (\sigma_2 - \sigma_3)^2 + (\sigma_3 - \sigma_1)^2]} \quad \text{Equivalent (von Mises) stress}$$

in terms of principal stresses, respectively.

In a first approach, the commonly used models can be separated by phenomenological models such as the Johnson-Cook criterion, and micromechanical models such as the Gurson model.

The **Johnson-Cook** criterion [1] describes a linear accumulation of damage, measured as the ratio of actual equivalent plastic strain to failure strain at a given triaxiality, temperature and strain rate. Since temperature changes are considered small for crash applications, temperature dependency is neglected here.

$$D = \int \frac{d\varepsilon_e^p}{\varepsilon_f} < 1 \quad \varepsilon_f = \left(d_1 + d_2 \exp\left(-d_3 \frac{\sigma_m}{\sigma_e}\right) \left[1 + d_4 \ln\left(\frac{\dot{\varepsilon}_e^p}{\dot{\varepsilon}_0}\right) \right] \right)$$

Based on test results, the equivalent fracture strain ε_f is a function of η to the negative power of triaxiality η . *Das η bedarf der Bezeichnung.*

The micromechanical model of **Gurson** [5], extended by Tvergaard and Needleman, describes ductile damage as nucleation, growth and coalescence of microvoids. Starting from an arbitrarily defined percentage of void volume in original state, void growth as the dominating damage mechanism is depending on the amount of hydrostatic pressure. The resulting dependency of equivalent fracture strain ε_f to triaxiality η cannot be described analytically in an easy way, as it can be for the Johnson-Cook model. For this reason, the equivalent fracture strains ε_f were calculated by means of numerical integration along paths of constant triaxiality η . The curve displayed in figure 2 is for ZStE340 deep-draw steel.

The forming limit diagram as depicted in figure 1a.) can - assuming isochoric plastic material behaviour - be transformed into the coordinates of ε_f and η as used in figure 2. Using this, a direct comparison of different failure models is possible:

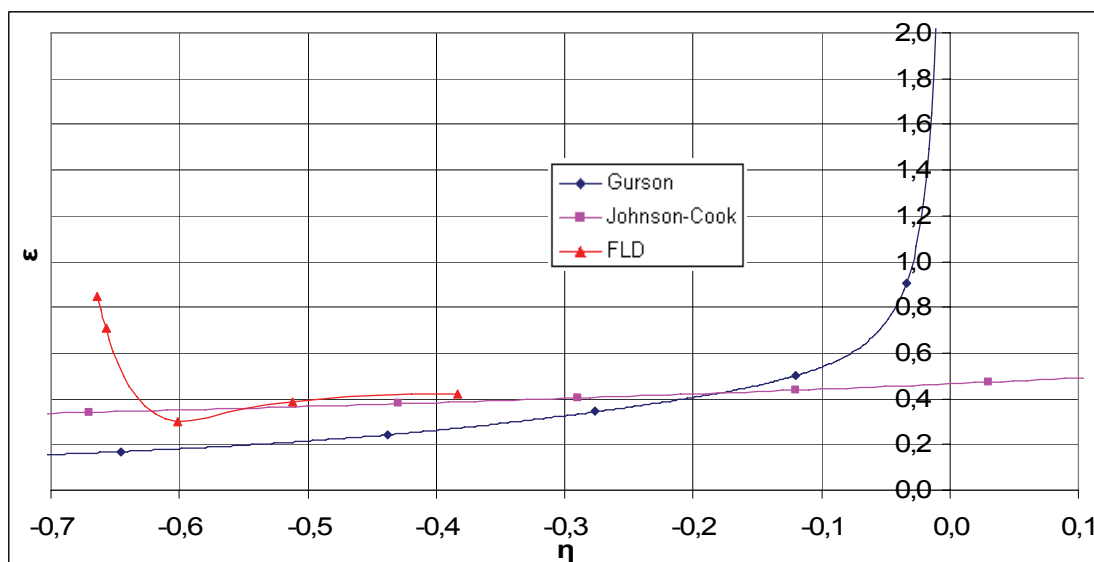


Figure 2: Equivalent failure strain ε_f vs. triaxiality η ; Johnson-Cook, Gurson and FLD

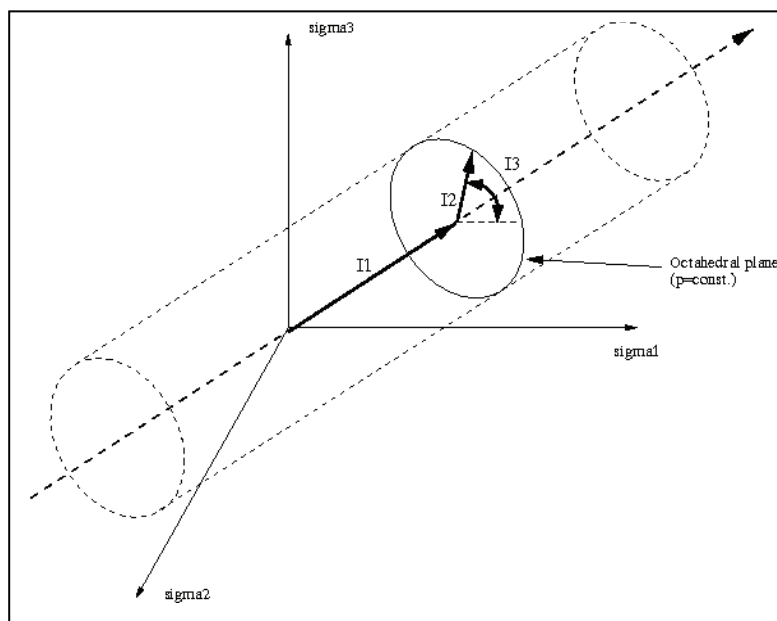
As can be seen in figure 2, both Johnson-Cook and Gurson models show a monotonic decrease of ε_f with increasing negative values of triaxiality.

The transformed FLD curve however shows – besides of differences in strain level – a principally different look, as it is not monotonically falling with increasing triaxiality. It actually shows a significant rise of failure strain for triaxialities above 0,6. These triaxialities represent the range of equi-biaxial tension, and are supposed to be the dominant stress state in stretch forming applications.

It seems that these failure criteria cannot directly be compared or transformed into each other. A description of equivalent failure strain depending on triaxiality alone seems to be insufficient, since the two concepts describe fundamentally different relationships between the two measures.

3 New concepts for the description of stress-state dependent damage

As indicated above, it seems evident that stress triaxiality alone is not a sufficient description for differences in stress states, as can be found between forming and crash loading. Besides of this, results of several experimental investigations by Wierzbicki and coworkers [3], Barsoum and Faleskog [7] and others are pointing into the same direction. In general, all possible stress states can be uniquely described by three invariants of stress tensor.



The three invariants defined in

terms of principal stresses :

$$I_1 = \sigma_1 + \sigma_2 + \sigma_3 = -3\sigma_m$$

$$I_2 = -(\sigma_1\sigma_2 + \sigma_2\sigma_3 + \sigma_3\sigma_1)$$

$$I_3 = \sigma_1\sigma_2\sigma_3$$

Figure 3: Invariants of stress tensor in principal stress space

By formulation of failure strains only depending on triaxiality $\eta = \sigma_m/\sigma_e$, which is a measure for the relation of 1st to 2nd invariant, there is no information about the third invariant. As shown in figure 3, the third invariant can be interpreted on the octahedral plane as the angle of deviatoric state with respect to the projected direction of first principal stress. This angle corresponds to the Lode angle, which is a commonly used deviation of the third invariant. By omitting this information about the deviatoric state, no difference is made between stress states having the same triaxiality. To overcome this, a deviatoric state parameter depending on the third invariant is considered.

3.1 Possible definitions of a deviatoric state parameter

Two different ways of describing deviatoric states are described in the following, since both have their advantages in their respective application.

3.1.1 Deviatoric state parameter based on complete stress tensor

This definition describes the third invariant of stress tensor in relation to σ_e to the power of 3.

$$\zeta = \frac{I_3}{\sigma_e^3} = \frac{\det(\underline{\underline{\sigma}})}{\sigma_e^3} = \frac{\sigma_1\sigma_2\sigma_3}{\sigma_e^3} \quad \text{in terms of principal stresses.}$$

Per definition, the third invariant I_3 equals zero for plane stress, as at least one principal stress is zero.

To get a better understanding of the meaning of this deviatoric state parameter, the range of possible values is investigated. For this purpose, the stress tensor in terms of principal stresses is written in a parametric form, with parameters a, b defined as

$$a = \frac{\sigma_2}{\sigma_1} \quad ; \quad b = \frac{\sigma_3}{\sigma_1} \quad \text{respectively.}$$

$$\sigma = \sigma_1 \begin{pmatrix} 1 & 0 & 0 \\ 0 & a & 0 \\ 0 & 0 & b \end{pmatrix}$$

with the range of definition for a and b resulting from the ordering of principal stresses:

$$1 \geq a \geq -\infty \quad ; \quad a \geq b \geq -\infty$$

One can find the envelope of all possible stress states in (η, ζ) space by looking at the extreme values of ζ . It can be shown that these values are reached for axis-symmetric stress states, meaning $a=b$. By solving the equations for ζ in η , two enveloping curves can be found describing ζ as a function of η by third-order parabolas. Both representing axis-symmetric stress states with $a=b$, the branching results from different signs.

$$\zeta_{axisymm.}^{\pm} = f(\eta) = -\eta^3 + \frac{1}{3}\eta \pm \frac{2}{27}$$

Another interesting state is represented by plane strain condition. As a fixed relation of a to b, one gets

$$b = 2a - 1 \quad \text{for plane strain.}$$

The corresponding function $\zeta(\eta)$ is

$$\zeta_{plane_strain} = f(\eta) = -\eta^3 + \frac{1}{3}\eta$$

In the resulting diagram, plane stress condition is described by the abscissa, in the range of

$$\frac{2}{3} \geq \eta \geq -\frac{2}{3}$$

An advantage of this deviatoric state parameter, in comparison to the second approach described below, is that the plane stress condition, as a common assumption in the simulation of sheet-metal forming, can conveniently be identified as ζ equals zero. As a disadvantage, the envelope of possible stress states as well as the plain strain condition is curved.

3.1.2 Deviatoric state parameter based on deviatoric stress tensor

For the reasons described above, another possible definition of a deviatoric state parameter was also taken into account. This definition has been proposed by T. Wierzbicki [2], [3]. The main difference is found in the fact, that it uses the third invariant of the deviatoric stress tensor, contrary to the complete stress tensor as discussed above.

$$\xi = \frac{27}{2} \frac{J_3}{\sigma_e^3} = \frac{27}{2} \frac{\det(\underline{s})}{\sigma_e^3} = \frac{27}{2} \frac{(\sigma_1 - \sigma_m)(\sigma_2 - \sigma_m)(\sigma_3 - \sigma_m)}{\sigma_e^3}$$

Due to this definition, ξ equals zero in plane strain conditions. Under plane stress conditions, there are only two non-zero principal stresses. Therefore, the third invariant of deviatoric stress tensor can be expressed as a function of first and second invariant. It was shown by T. Wierzbicki that ξ be expressed as function of triaxiality:

$$\xi = f(\eta) = \frac{27}{2} \eta \left(\eta^2 - \frac{1}{3} \right) \text{ for plane stress.}$$

The main difference in comparison to the formulation of ζ is that the range of possible stress states in (η, ξ) space appears as a rectangular area. Possible values of ξ are $1 \geq \xi \geq -1$.

3.2 Maps of possible stress states

To get an impression of the differences between both parameters, the possible values and their respective mechanical meaning are displayed below:

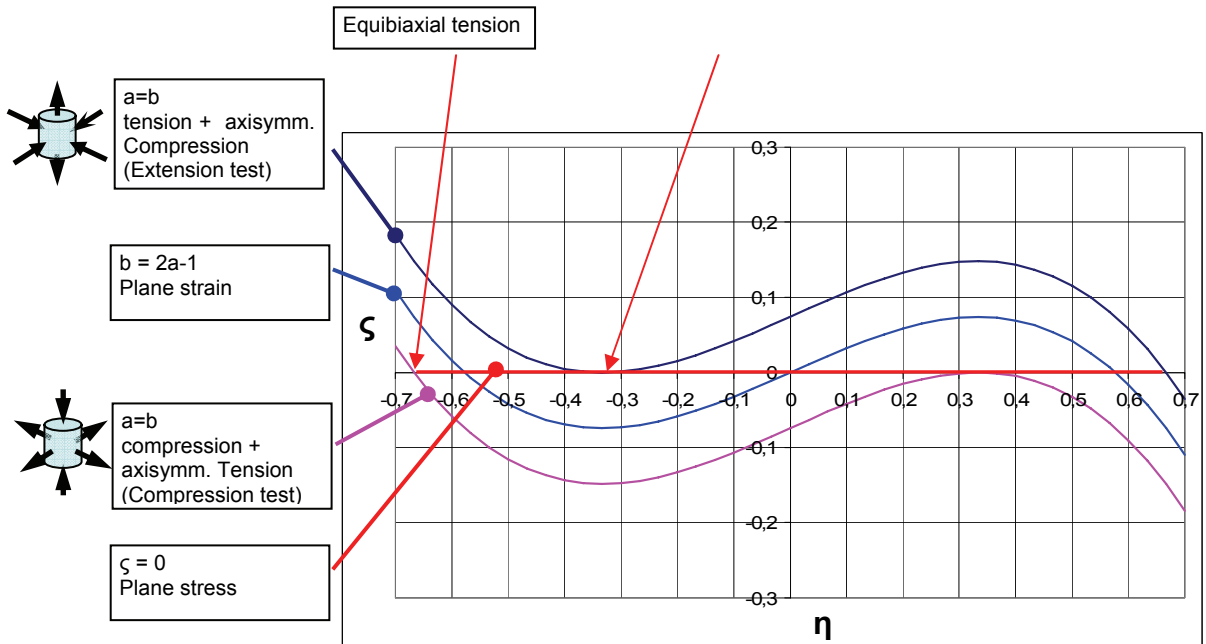


Figure 4: Map of possible stress states in (η, ζ) space

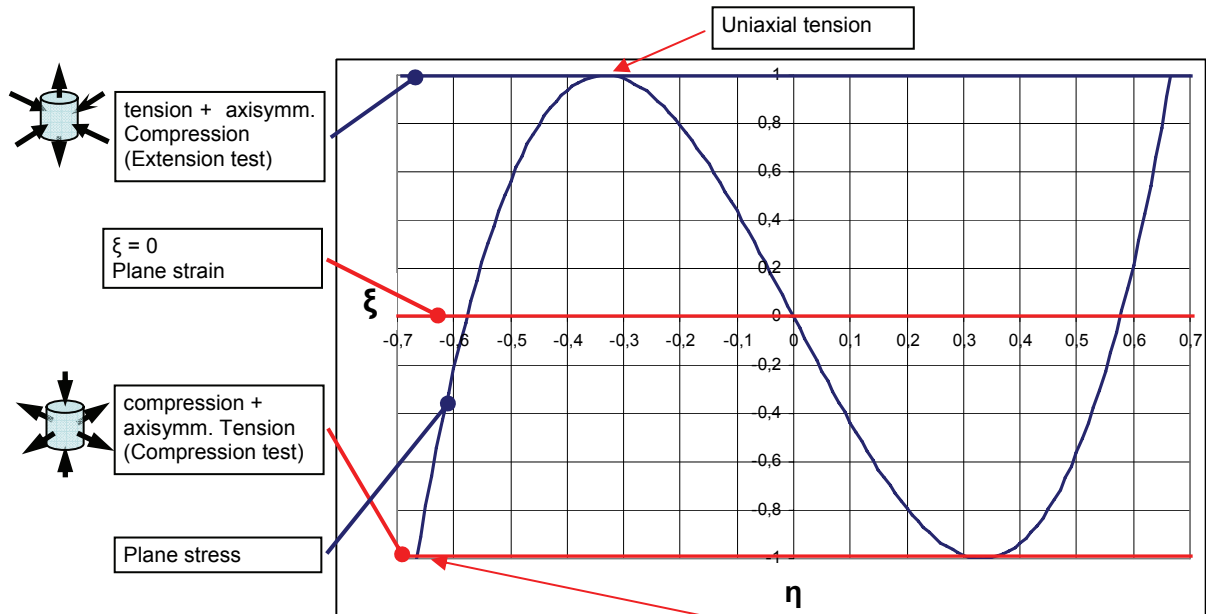


Figure 5: Map of possible stress states in (η, ξ) space

As can be seen from figures 4 and 5, both definitions of a deviatoric state parameter describe the same mechanical relations. ζ can be described by ξ following a simple transformation of coordinates, and vice versa.

3.3 Effects of deviatoric state on failure strain

As can be seen in figures 4 and 5, stress states having the same triaxiality η can be of fundamentally different nature. So, for example, a value of $\eta = -1/3$ corresponds to uniaxial tension in plane stress conditions. If the stress state is not plane, other possible load cases with the same triaxiality are plane strain ($\zeta = -2/27$), or compression combined with axisymmetric tension ($\zeta = -4/27$). It seems obvious that differences in equivalent failure strain can be expected between these load cases. Generally, a minimum failure strain can be expected for plane strain conditions. Considering this, a definition of failure strains as a surface in coordinates of (η, ζ) or (η, ξ) seems necessary.

Since the shape of the area of possible stress states is rectangular for Wierzbicki's formulation of ξ , and the values of ξ are limited to the range of -1 to 1, this formulation is preferred for the definition of a failure surface. As can be seen from its definition, ζ is growing without a limit for $\eta \rightarrow \pm\infty$.

3.4 Considerations about failure surface shape

In recent years, several investigations about a Lode-dependent failure surface have been published. Among them are Wierzbicki [2], [3] and Xue [4], which have considered possible surface shapes based on test results and theoretical investigations. Starting with a formulation symmetric to the plane $\xi = 0$, in later publications an asymmetric failure surface with respect to the ξ - plane is proposed. Based on experimental data of aluminium Al-2024, it is seen that failure strains for negative values of ξ are smaller than for positive values of ξ . This also corresponds to the micromechanical idea of the Gurson model, which implies that hydrostatic pressure in tension is propagating weakening and failure. Hydrostatic compression may even prevent failure at sufficiently high values [4].

The shape of the curves that result from cuts through the surface at constant values of ξ , is that of a monotonically decreasing function of η . Similar to the principal shape of failure strain curves according to the Johnson-Cook failure criterion [1], a function of e to the negative power of η could be used for this definition (see also figure 2).

One thinkable means of a Lode-dependent failure criterion, would therefore be to extend the Johnson-Cook criterion with its principle of linear damage accumulation by a Lode-dependent term. Depending on the desired shape and asymmetry of the failure surface, a power law function of ξ can be used to model the dependency in ξ - direction.

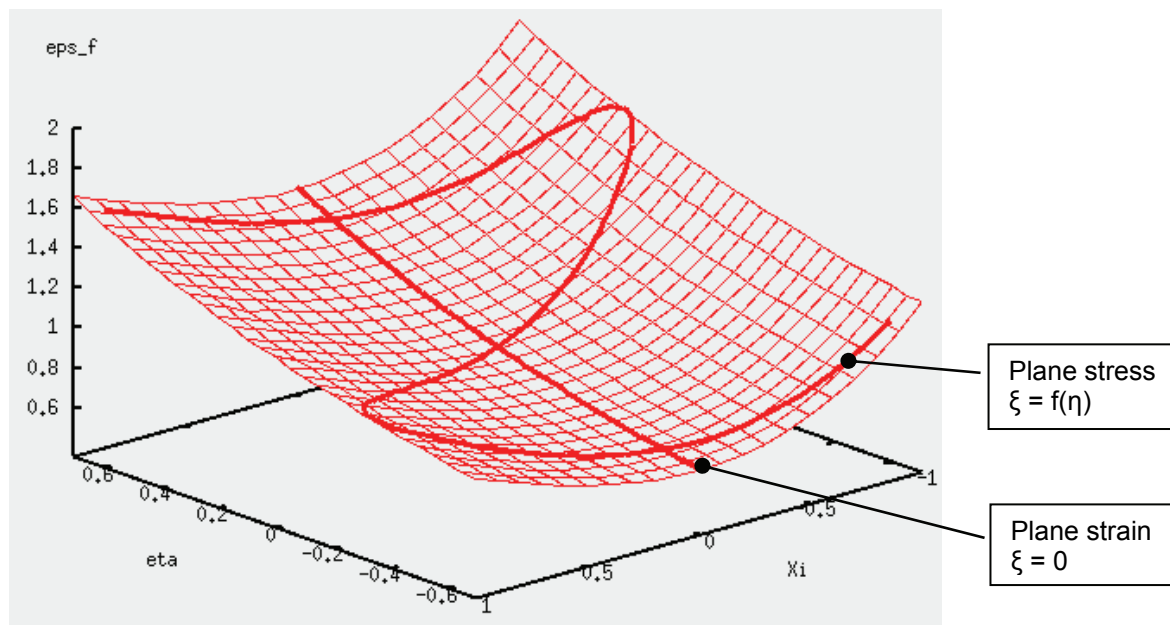


Figure 6: Example of failure surface in (η, ξ) coordinates defined by an extended Johnson-Cook criterion

Looking at the Gurson model with modifications by Tvergaard and Needleman [5], it is obvious that damage accumulation is considered non-linear here. By reaching a critical value of pore volume

fraction f_c , a damage parameter f^* is assigned a value of f multiplied by a factor. Being a measure of damage rather than a physical pore volume fraction, the onset of coalescence or necking should be modelled with this formulation. Consequently, the accumulation of damage is becoming non-linear, since - starting from f_c - damage accumulation is being accelerated.

Another possible way of non – linear damage accumulation was proposed by Xue [4]. Here, damage accumulation is described by a power law damage rule.

A general assumption in the works cited above is that damage is treated as a scalar quantity. For fairly isotropic materials such as deep – draw steels, this assumption seems rather reasonable, while tensorial formulations of damage would add quite some complexity to a model. Furthermore, the transfer of damage data in the process chain would be made even more difficult, due to different meshes used in forming and crash simulations.

4 Stress states in Nakazima tests

To get an idea of the stress states occurring in the tests used for determination of Forming Limit Diagrams (FLDs), the most common method for this is investigated in the following. Usually, Nakazima experiments using several differently sized cut-outs from the ideally round shaped blank are used. Blanks with varying width in the middle section are held in a circular drawbead. The specimen is then deep-drawn using a hemispherical punch until cracking occurs. The shape of these blanks was adapted from the draft standard ISO 12004 [6], and only one quarter is modelled here due to symmetry.

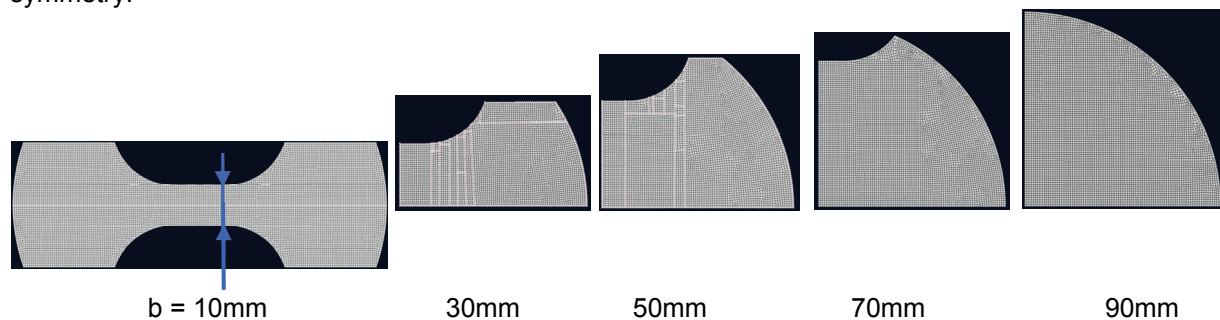


Figure 7: Quarter models of blanks with different widths for Nakazima tests

Triaxialities are usually ranging from nearly uniaxial tension for small widths to equi-biaxial tension for greater widths. In order to allow for an identification of occurring stress states, a full 3D – discretization using solid elements was necessary. By using shell elements, stress states would be limited to plane stress by the underlying shell assumption; except that out of plane shear stresses existing in some shell formulations. Using a blank thickness of 1mm, 5 layers of fully integrated brick elements with an average edge length of 0.5mm were used. For reference purposes, all blanks were also modelled using fully integrated shell elements with the same meshes. This was to identify the differences in results due to the shell-formulation enforced plane stress conditions.

Special attention was laid on the determination of applicability of plane stress conditions on these tests. Since sheet metal tests are usually modelled with shell elements, it was to be pointed out if plane stress is an applicable assumption for these tests.

4.1 Results from computations

As an important measure of the stress state, the triaxiality η throughout the tests is displayed for both solid and shell element tests. The elements considered were chosen at the same location near the centre of the punch, for the solid models the middle element in thickness direction was chosen.

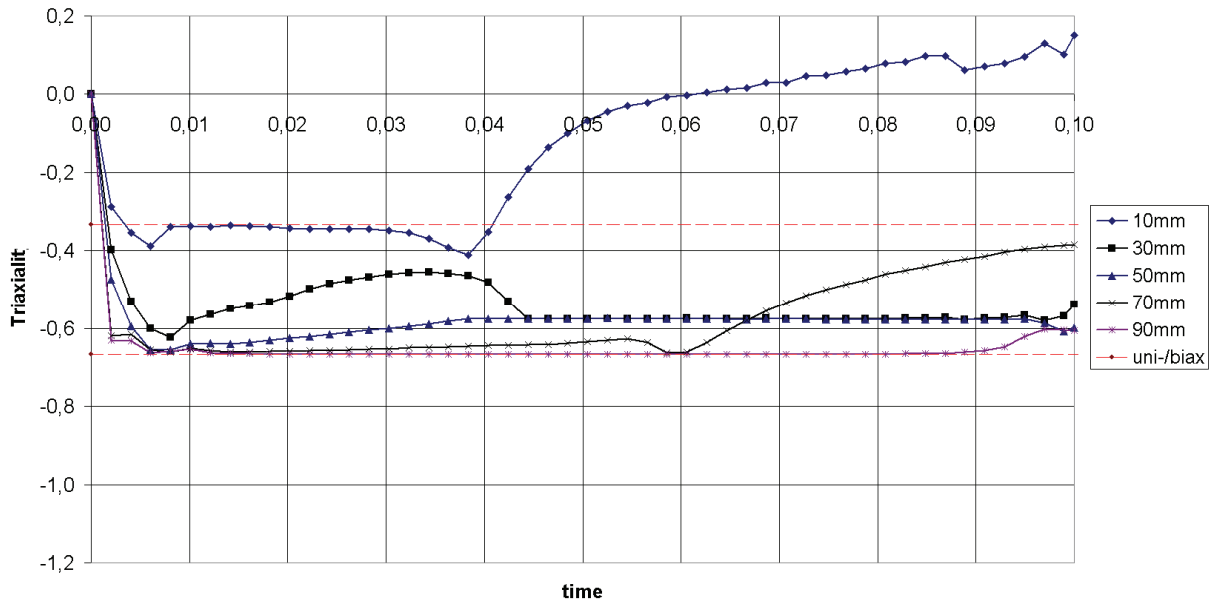


Figure 8: Triaxiality η vs. time for shell element Nakazima tests

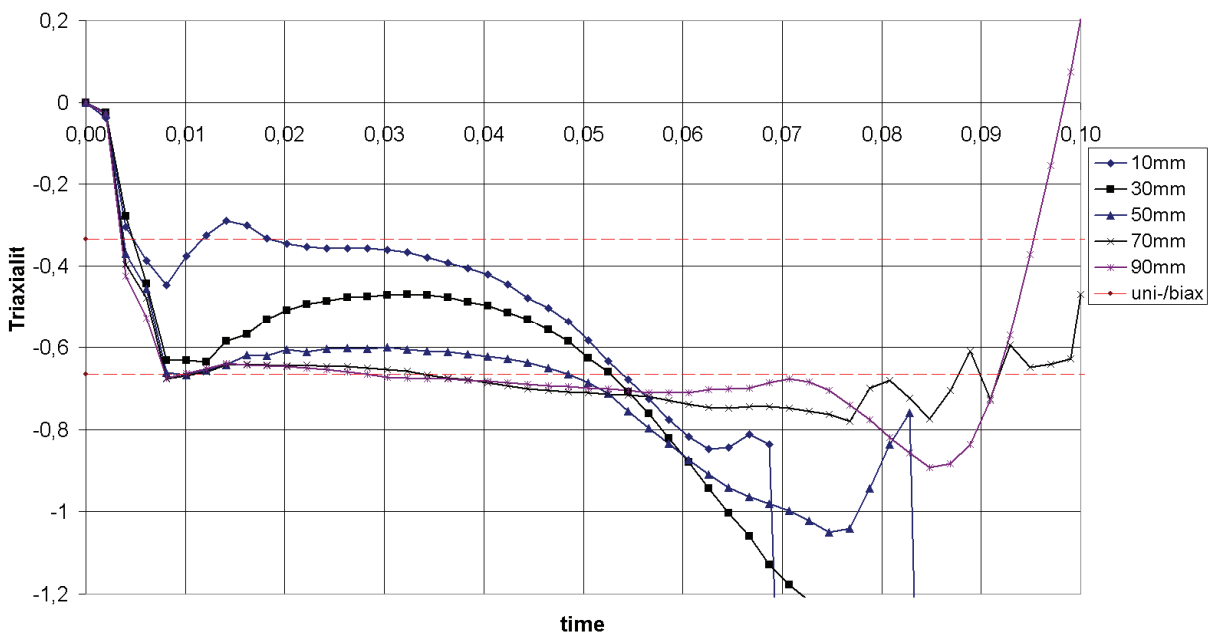


Figure 9: Triaxiality η vs. time for solid element Nakazima tests

The shell formulation enforces plane stress conditions (figure 8). By looking at the results of the solid element formulation (figure 9), it can be clearly seen that triaxialities are not constant at all throughout the test. Another interesting observation is that especially the narrower tests are clearly leaving plane stress conditions to some extent, since smaller triaxialities than $-2/3$ are violating the plane stress definition.

To get a better impression of the applicability of the plane stress conditions, the deviatoric state parameter ζ was printed for the same solid elements as in figure 8 and 9. Since in these tests no compressive stresses occur, only one half of the diagram shown in figure 4 is used. Displayed as an example is the specimen with a width of 30mm. All other blank widths show similar curves.

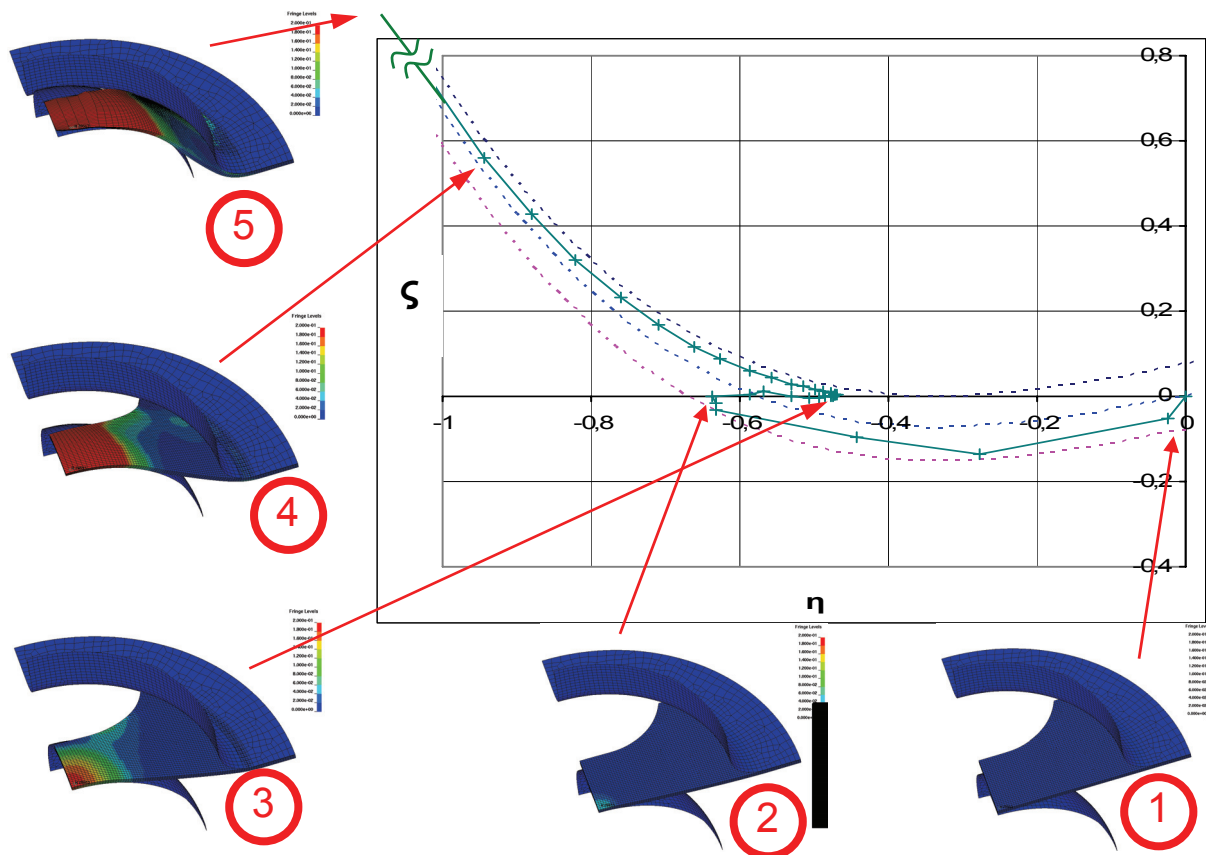


Figure 10: Deviatoric state parameter during Nakazima test, 30mm blank width

As can be seen from figure 10, the stress state of the test is plane stress only between states nr. 2 and 3 ($\zeta = 0$). Showing plane stress, triaxiality is changing continuously here. Punch displacement in state nr. 3 is about 10mm. Maximum equivalent plastic strain in this state is about 20%. For increasing displacement and strain, the deviatoric state parameter is following a line of constant ratio of 2nd to 3rd principal stress.

As a result of these calculations, it can be noted that triaxiality in Nakazima tests is following a rather complex loading history. Constant stress states – especially for narrow specimen widths – not provided. The assumption of plane stress conditions is justified only for small elongations and strains.

5 Conclusions

With results from these calculations, possible explanations for the differences in failure criteria of forming and crash simulations are in reach. Using a definition of failure strain as a surface in (η, ζ) or (η, ξ) area leads to different failure strains for stress states with the same triaxiality but different values of ζ or ξ .

Furthermore, the calculations show that the Nakazima tests having a full circle blank shape, thus leading to triaxialities of about $-2/3$, are sticking to plane stress conditions quite long in comparison to those with lower triaxialities. This leads to an explanation for the differences in shape of failure curves: the biaxial bulge tests show significantly higher failure strains, since the ξ - value corresponding to a triaxiality of $\eta = -2/3$ is $+1$ for plane stress. Because of this, the stress state is lying on a curve of high failure strains, representing an axis-symmetric stress state.

The curves of failure strain as a function of η that are used for ballistic and crash purposes are often measured using specimen that did not necessarily show plane stress conditions. Consequently, measured failure strains may differ from values corresponding to plane stress conditions. In addition, equi-biaxial tension tests are quite difficult to conduct using sheet metal specimen. Because of this, values of failure strain for stress states near $\eta = -2/3$ are often extrapolated from uniaxial tension tests. A common assumption for this extrapolation is a monotonic decrease of failure strain with triaxiality, which leads to an underestimation of failure strains for equi-biaxial loading.

As a result of this, a consistent formulation of failure strains in (η, ξ) space, as was proposed by Wierzbicki [2] and others, seems necessary. To define such a failure surface, a greater number of tests with characteristic values of η and ξ is needed. Special attention has to be laid on constant stress states throughout the tests. Possible formulations for the dependency of failure strains on the third invariant have to be evaluated by further experimental and theoretical investigations. To be able to describe the behaviour of different classes of high strength steels, and other materials such as aluminium, a material model showing great flexibility has to be developed. One possibility for this is an extension of the Johnson-Cook model as described above, which is quite similar to the model proposed by Wierzbicki [2], and Xue [4]. Another possibility is an extension of the micromechanical Gurson model, as has been proposed recently by several authors.

Further investigations are also necessary on possible nonlinear damage accumulation and suitable formulations for this. Another issue regarding differences between forming and crash simulations is a possible influence of different strain rates, which was not taken care of in this work. Solving these issues could therefore lead to a consistent and continuous material formulation suitable for both forming and crash applications in the future.

6 References

- [1] Johnson, G.R., Cook, W.H., (1985): "Fracture characteristics of three metals subjected to various strains, strain rates, temperatures and pressures", Engineering Fracture Mechanics, vol.21, No.1, pp. 31-48
- [2] Wierzbicki, T., (2007). "Fracture of AHSS Sheets – Addendum to the Research Proposal on Fracture of Advanced High Strength Steels", Impact and Crashworthiness Laboratory, Massachusetts Institute of Technology
- [3] Wierzbicki, T., Bao, Y., Lee, Y.-W., Bai, Y., (2005): "Calibration and evaluation of seven fracture models", Int. Journal of Mechanical Sciences, vol.47, pp. 719-743
- [4] Xue, L., (2007): "Damage accumulation and fracture initiation in uncracked ductile solids subject to triaxial loading", Int. Journal of Solids and Structures, vol.44, pp. 5163-5181
- [5] Feucht, M., (1999). "Ein gradientenabhängiges Gursonmodell zur Beschreibung duktiler Schädigung mit Entfestigung". Dissertation, TU Darmstadt, Institut für Mechanik
- [6] ISO/WD 12004, (2004): "Metallic Materials – Determination of forming limit curves", Preparatory Standard, International Organization for Standardization
- [7] Barsoum, I., Faleskog, J., (2006): "Rupture mechanisms in combined tension and shear – Experiments", Int. Journal of Solids and Structures vol.44, pp. 1768-1786

